Carbon Letters
https://doi.org/10.1007/s42823-024-00779-1

Online ISSN 2233-4998
Print ISSN 1976-4251

ORIGINAL ARTICLE

Effect of asphaltene content in petroleum residues on carbon layer properties and the electrochemical performance of SiOx as an anode in lithium-ion batteries

KyungSoo Kim[1] · In Woo Lee[1] · Yebin Lee[2] · Yongcheol Choi[2] · Young-Seak Lee[1,3]

Received: 30 April 2024 / Revised: 11 July 2024 / Accepted: 13 July 2024

Abstract
In this study, carbon coating was carried out by physical vapor deposition (PVD) on SiO_x surfaces to investigate the effect of the deposited carbon layer on the performance of lithium-ion batteries as a function of the asphaltene content of petroleum residues. The petroleum residue was separated into asphaltene-free petroleum residue (ASF) and asphaltene-based petroleum residue (AS) containing 12.54% asphaltene by a solvent extraction method, and the components were analyzed. The deposited carbon coating layer became thinner, with the thickness decreasing from 15.4 to 8.1 nm, as the asphaltene content of the petroleum residue increased, and a highly crystalline layer was obtained. In particular, the SiOx electrode carbon-coated with AS exhibited excellent cycling performance with an initial efficiency of 85.5% and a capacity retention rate of 94.1% after 100 cycles at a current density of 1.0 C. This is because the carbon layer with enhanced crystallinity had sufficient thickness to alleviate the volume expansion of SiOx, resulting in stable SEI layer formation and enhanced structural stability. In addition, the SiOx electrode exhibited the lowest resistance with a low impedance of 23.35 Ω, attributed to the crystalline carbon layer that enhanced electrical conductivity and the mobility of Li ions. This study demonstrated that increasing the asphaltene content of petroleum residues is the simplest strategy for preparing SiOx@C anode materials with thin, crystalline carbon layers and excellent electrochemical performance with high efficiency and high rate performance.

Keywords Lithium-ion batteries · SiOx · Carbon coating · Petroleum residue · Asphaltene

1 Introduction

Due to global warming and environmental pollution, there is increasing interest in using electric vehicles and energy storage systems (ESSs) as eco-friendly energy storage devices in response to climate change, and the development of lithium-ion batteries (LIBs) is becoming increasingly important. Li-ion batteries are widely used because of their high energy and power density, long cycle life and stability, and low cost [1–3]. In particular, carbon anode materials such as graphite are widely used as anode materials for Li-ion batteries, but they have limited theoretical capacity (372 mAh/g) [4–7]. However, to meet the market demand for electric vehicles, it is necessary to improve the electrochemical properties, such as the capacity and rate capability, by increasing the energy density and charging rate of LIBs [8–11].

Silicon has been investigated as a next-generation anode material due to its high theoretical capacity (~4200 mAh/g), low operating potential, and natural abundance [12, 13]. However, during charge/discharge cycling, silicon has high volume expansion (~300%) due to the insertion and delocalization of lithium ions, which contributes to the structural collapse of silicon particles and the repeated formation of a solid electrolyte interface (SEI) layer [14]. In addition, the intrinsic conductivity of silicon is limited by its semiconductor properties, resulting in low active particle utilization and poor high-rate capability [15]. Therefore, SiOx materials have been widely investigated as silicon substitutes in recent years [16–19]. SiOx has a relatively small volume

✉ Young-Seak Lee
youngslee@cnu.ac.kr

[1] Department of Chemical Engineering and Applied Chemistry, Chungnam National University, Daejeon 34134, Republic of Korea

[2] Carbon Materials R&D Center, POSCO MC Materials, Gwangyang 57812, Republic of Korea

[3] Institute of Carbon Fusion Technology (InCFT), Chungnam National University, Daejeon 34134, Republic of Korea

Published online: 24 July 2024

expansion (150%) compared to silicon, and it can be alloyed with lithium ions to form Li_2O and Li_xSiO_n to act as a matrix to buffer volume expansion during charging and discharging, but its low electrical conductivity and large volume expansion limit its practical application [20]. Therefore, in recent years, various carbonaceous materials have been studied to mitigate the volume expansion of SiOx and improve its electrical conductivity to improve its performance [21–26]. These carbonaceous materials are known to mitigate the volume expansion of SiOx materials and have been fabricated in the form of various structures, such as core–shell [21], hollow [22], 3D porous [23], yolk–shell [24], and surface coating [25, 26] structures, to act as conductive networks that facilitate electron and ion transport [27, 28]. Among the various carbon structures, carbon coatings on silicon surfaces have been investigated, but there is little research on the unique properties of carbon precursors. To improve the electrochemical performance of LIBs, it is important to have a good understanding of how the microstructure of the carbon layer formed by carbon precursors of various compositions affects the electrochemical behavior of LIBs.

Carbon coating methods such as wet coating using solvents [29], chemical vapor deposition (CVD) using gases [30], and physical vapor deposition (PVD) [31] have been widely studied for forming carbon coatings on SiOx surfaces. Among the various coating methods, there is increasing interest in the PVD method based on petroleum residues to form carbon coatings on SiOx surfaces; the advantages of this method include the cost benefits of using petroleum residues as carbon precursors and a lack of mechanical damage to SiOx [32]. In addition, petroleum residue is generated as a byproduct of the refining process of Korean oil companies, and it is necessary to explore value-added processes for utilizing these residues [33–36]. Therefore, coating SiOx with petroleum residue can add high value and yield economic benefits. To take advantage of these benefits, Lee et al. modified petroleum residues by adjusting the evaporation temperature, prepared SiOx/C by PVD-coating the SiOx surface, mixed the prepared material with graphite and reported the electrochemical properties of the composite [37]. They investigated the aromatic composition of petroleum residue as a function of evaporation temperature and confirmed the effect of the crystal structure and thickness of the carbon coating layer on electrochemical performance. However, it is difficult to control the composition of petroleum residue during reforming through evaporation, and it is difficult to determine the effect of petroleum residue composition on the SiOx coatings.

It is important to study how the composition of petroleum residues, which are carbon precursors, affects carbon coating development. In general, the composition of petroleum residues can be altered via extraction with solvents such as hexane, toluene, tetrahydrofuran, and quinoline to achieve a narrow molecular weight distribution and similar composition [38]. Saturated and aromatic hydrocarbons are represented by relatively low molecular weight fractions, while resins and asphaltenes can be distinguished by high molecular weight fractions [39]. Therefore, in this study, to investigate the effect of petroleum residue asphaltene content on carbon layer formation on SiOx surfaces, the asphaltene content of petroleum residues was altered, and these residues were utilized to prepare carbon-coated SiOx by the PVD carbon-coating method. The crystal structure and thickness of the carbon layer were analyzed, and the effect of the layer on electrochemical performance was confirmed. This study investigated the effect of petroleum residual asphaltene content on the SiOx carbon coating layer and electrochemical performance.

2 Experimental

2.1 Materials

In this study, petroleum residue samples classified according to the asphaltene content were used, and they were obtained from POSCO MC Materials and named ASF, DO, and AS with increasing asphaltene content. The supplied petroleum residue is DO (FCC-DO, SK innovation, Korea), and ASF (asphaltene-free petroleum residue with 0% asphaltene content) was obtained by dissolving asphaltene components in DO (asphaltene content of 0.63%) using n-heptane solvent and then removing asphaltene components using a centrifuge [40]. AS (asphaltene-based petroleum residue with asphaltene content of 12.54%) was obtained by dissolving the low molecular weight components of DO using n-hexane solvent to increase the asphaltene content, and then removing the low molecular weight components by centrifugation [41, 42]. The petroleum residues with different asphaltene contents were used as the carbon layer precursors. SiOx (Daejoo, Korea, 5 μm) and graphite (MAG, Hitachi Kasei, Japan, 25 μm) were used as anode materials for the electrodes. Carbon black (Super-P Li, Timcal Ltd.) was used as a conductive material. Carboxymethylcellulose (CMC, MTI, Korea) and styrene-butadiene rubber (SBR, 50 wt%, MTI, Korea) were used as binders.

2.2 Preparation of SiOx coated with petroleum residual oil with different asphaltene contents

Carbon coating of SiOx with petroleum residue was performed by depositing 1 g of SiOx and 5 g of petroleum residue with different asphaltene contents at 400 °C for 1 h at a ramp rate of 5 °C/min in a nitrogen atmosphere, followed by carbonization at 950 °C for 2 h at a ramp rate of 10 °C/min [31]. The as-prepared carbon-coated SiOx samples were

named SiOx@C_ASF, SiOx@C_DO, and SiOx@C_AS according to the asphaltene content of the petroleum residue.

2.3 Material characterization

The thermal behavior of the petroleum residues during pyrolysis and the content of the carbon coating layer of SiOx were characterized by thermogravimetric analysis (TGA, METTLER TOLEDO) to compare the pyrolysis behavior of the residues with different asphaltene contents. Elemental analysis (EA, Flash 2000 and EA1112, Thermo Fisher Scientific) was performed to analyze the elemental composition and H/C ratio of the petroleum residues. In addition, saturated, aromatic, resin, and asphaltene analysis (SARA) was performed using the thin-layer chromatography–flame ionization detection (TLC–FID) method to identify the composition of petroleum residues with different asphaltene contents. X-ray diffraction (XRD, Bruker D8 ADVANCE, USA) and Raman analysis (LabRAM HR-800, Horiba, Japan) were performed with a laser at 514 nm to determine the crystal structure of SiOx coated with petroleum residues with different asphaltene contents. X-ray photoelectron spectroscopy (XPS, K-Alpha+, Thermo Scientific, USA) analysis with Al Kα radiation was performed to investigate chemical bonding in the SiOx coated with petroleum residues with different asphaltene contents. In addition, transmission electron microscopy (TEM, Tencai G2 F30, FEI, USA) images were obtained to characterize the microstructure and thickness of the carbon layer on the carbon-coated SiOx.

2.4 Electrochemical measurements

The following electrode slurry was prepared to evaluate the electrochemical properties of the manufactured carbon-coated SiOx. The slurry was prepared by mixing the prepared active anode material, carbon black, and aqueous binder in a weight ratio of 8:1:1 in a Thinky mixer. The electrode's loading level was 6–7 mg/cm^2. This slurry was then coated on copper foil at a thickness of 200 µm using a bar-coating method and dried in a vacuum oven at 100 °C for 8 h. The electrolyte was prepared by mixing 1 M $LiPF_6$, ethylene carbonate (EC), diethyl carbonate (DEC) (1:1 vol), and 10 wt% additive fluoroethylene carbonate (FEC). The coin cells were fabricated using Li metal as a counter electrode in a glove box under an Ar atmosphere. To evaluate the electrochemical properties of the fabricated cells, a multichannel battery cycler (PNE Solution, Korea) was used to analyze the cycling stability and rate performance of the cells at 0.005–2.5 V drive voltages. Cycling stability was analyzed over 100 cycles at 1 C for charge and discharge, and the rate characterization was performed by varying the current density with C rates of 0.2, 0.5, 1, 2, 5, and 0.2 C to verify the rate performance. Electrochemical impedance spectroscopy (EIS) measurements were performed by a Gamry Interface 1000E workstation in the frequency range of 0.01–10^6 Hz.

3 Results and Discussion

3.1 Characterization of residues with different asphaltene contents

The proportions of major components of the petroleum residues with different asphaltene contents were determined by using TLC–FID to evaluate the proportions of the SARA components, as shown in Fig. 1a. The ASF had components similar to that of the DO. Nevertheless, it was observed that the proportion of the saturated component increased due to the removal of asphaltenes by the conventional solvent extraction method. On the other hand, AS was composed of fewer saturated and aromatic components than DO due to the removal of saturated components by the solvent extraction method, which increased the asphaltene content to 12.54%. It was concluded that the asphaltene content of petroleum residues could be controlled by the solvent extraction method and that the asphaltene content determined the overall molecular weight of the petroleum residues. ASF was composed of low-molecular-weight components with high saturation and aromatic content, and asphaltenes were removed. In contrast, AS was composed of higher molecular weight components than DO due to its higher asphaltene content and lower saturated and aromatic content [43]. In general, it is known that carbon growth during the thermal treatment of petroleum residues is affected by the molecular weight composition of the residues, especially the asphaltene content, which affects coke formation [44].

TGA and DTG were performed to investigate the pyrolysis behavior of the petroleum residues from room temperature to 1000 °C under a nitrogen atmosphere, and the results are shown in Fig. 1b-c. Figure 1b shows that ASF and DO decreased in weight at approximately 130 °C, while the weight of AS decreased at approximately 154 °C. Furthermore, the final residues amounted to 0.23 wt% and 1.42 wt% for ASF and DO, respectively, while AS had a final residue of 22 wt%. In general, petroleum residue is composed of various aliphatic hydrocarbons and aromatic hydrocarbons [45, 46]. Therefore, in petroleum residue, aliphatic hydrocarbons and low-molecular-weight hydrocarbons such as benzene and naphthalene are evaporated by heat, followed by the evaporation of polymeric hydrocarbons with three or more rings. The weight loss in AS started at a temperature 24 °C higher than that of ASF and DO. The final residue of AS was approximately 99 times greater than that of ASF, suggesting that AS was composed of polymeric hydrocarbons because the weight loss occurred at a higher temperature, and the final residue was much greater than that of

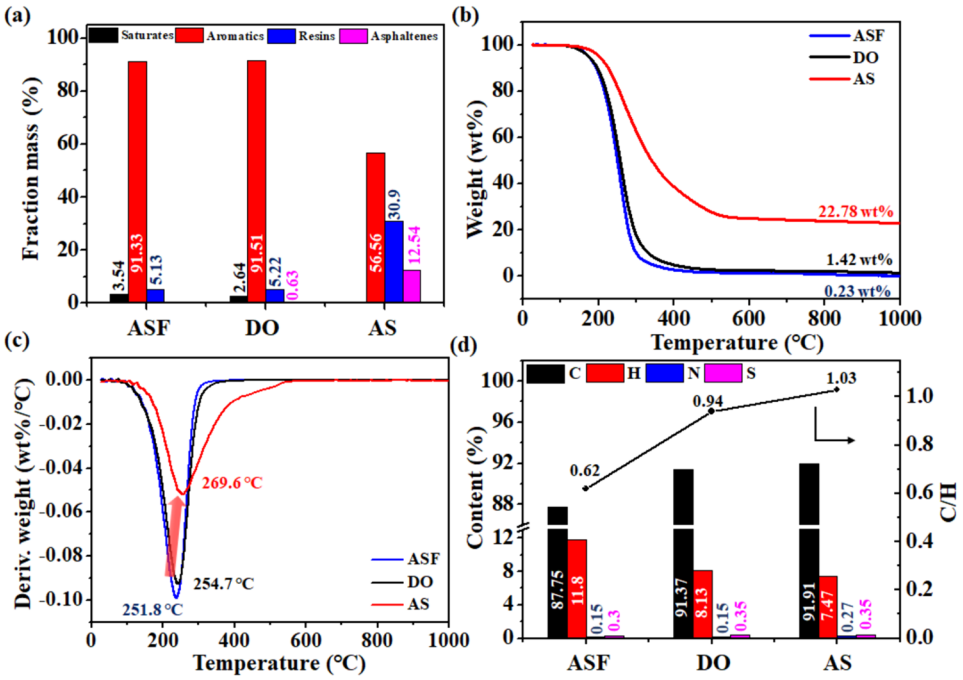

Fig. 1 (**a**) SARA analysis, (**b**) TGA curve, (**c**) DTG curve, and (**d**) elemental analysis of ASF, DO, and AS

other samples. Figure 1c shows that the DTG curve had a single peak for all samples. ASF peaked at 251.8 °C, and with increasing asphaltene content, the peak shifted to the right to 254.7 °C for DO and 269.6 °C for AS. This confirms that an increase in the asphaltene content of petroleum residues is associated with an increase in high-molecular-weight components. Previous studies have shown that polymeric hydrocarbons such as dicyclic and tricyclic aromatic hydrocarbons undergo condensation-based polymerization reactions to form carbon layers with improved crystallinity more readily than low-molecular-weight hydrocarbons such as monocyclic aromatic hydrocarbons and aliphatic hydrocarbons [47]. The elemental contents of petroleum residues with different asphaltene contents were investigated and are shown in Fig. 1d. AS had a lower carbon and hydrogen content than ASF, but its hydrogen content was significantly reduced, resulting in a lower H/C ratio. The lower H/C ratio suggested that AS was composed of more aromatic polymeric hydrocarbons. Therefore, we determined the effect of these polymeric hydrocarbons on the carbon layer formed during carbon-coating on SiOx.

3.2 Characterization of carbon-coated SiOx with different asphaltene contents

XRD and Raman analysis were performed to characterize the structural properties and crystallinity of the carbon layer formed on SiOx with petroleum residues containing different asphaltene contents, and the results are shown in Fig. 2. Figure 2a shows the XRD analysis of the SiOx and carbon-coated SiOx. The SiOx peaks are characterized by crystalline nano silicon peaks at (111), (220), and (311), and a broad amorphous SiO_2 peak is observed between 20° and 25° [48]. The carbon-coated SiOx samples had peaks

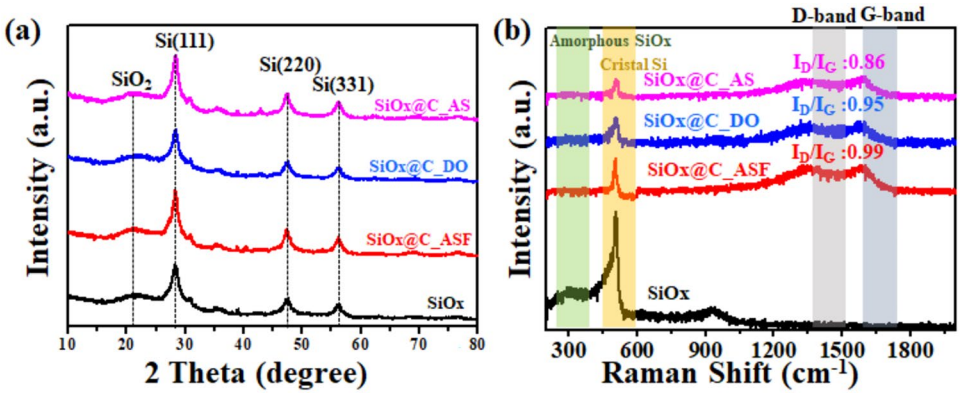

Fig. 2 (**a**) XRD patterns of SiOx, SiOx@C_ASF, SiOx@C_DO, and SiOx@C_AS and (**b**) Raman scattering patterns of SiOx, SiOx@C_ASF, SiOx@C_DO, and SiOx@C_AS

similar to those in SiOx, which appeared to arise from superposed amorphous SiO_2 peaks and amorphous carbon peaks. It is believed that the carbon layer formed an amorphous structure due to the low annealing temperature (less than 1000 °C). Figure 2b shows the Raman spectra of SiOx and carbon-coated SiOx analyzed with a laser of 514 nm in the range of 200–2000 cm^{-1}. In the Raman spectra, D (1340 cm^{-1}) and G (1580 cm^{-1}) peaks are observed, in which the D peak is related to defects in the carbon and the G peak is related to the crystallinity of the carbon [49]. The I_D/I_G value of SiOx@C_DO was approximately 0.95, while those of SiOx@C_ASF and SiOx@C_AS were 0.99 and 0.86, respectively. The I_D/I_G values of all the samples were greater than 0.8, which indicated that the carbon layer formed on the SiOx surface had an amorphous structure [49]. Furthermore, SiOx@C_ASF had the highest I_D/I_G value, while SiOx@C_AS had the smallest I_D/I_G value. Since a smaller I_D/I_G indicates a more crystalline structure, SiOx@C_AS was determined to have a more crystalline structure than the other materials. This is because high-molecular-weight hydrocarbons such as asphaltenes can yield a more crystalline structure than low-molecular-weight hydrocarbons during the carbon coating process, and low-molecular-weight hydrocarbons are evaporated and removed during the carbon coating process, resulting in a disordered structure [50]. A comparison of the crystalline Si peaks of these three samples during carbon coating shows that the intensity of the crystalline Si peaks was proportional to the asphaltene content of the deposited residue. This suggests that the higher the asphaltene content of the residue (ASF < DO < AS), the thinner the carbon layer on SiOx, so the intensity of the Si peak was relatively high. In addition, the deposited carbon coating layer had defects due to decomposition upon heat treatment. AS with a larger asphaltene content in the residue resulted in fewer defects than ASF with a smaller asphaltene content in the residue. It is believed that a residue with low asphaltene content can have a detrimental effect on the layer properties by resulting in more defects during heat treatment, even when the carbon layer is thick. In other words, polymeric hydrocarbons such as asphaltenes evaporate under the same carbon coating conditions and, therefore, have low mobility but can be easily condensed and polymerized during heat treatment, which is believed to improve the crystallinity of the carbon layer.

To investigate the elemental composition and surface chemical bonding of the carbon coating on SiOx coated with petroleum residues with different asphaltene contents, XPS analysis was performed, and the results are shown in Fig. 3. In Fig. 3a, Si 2p, Si 2s, C 1s, and O 1s peaks are observed, corresponding to binding energies of 103.0, 155.0, 284.0,

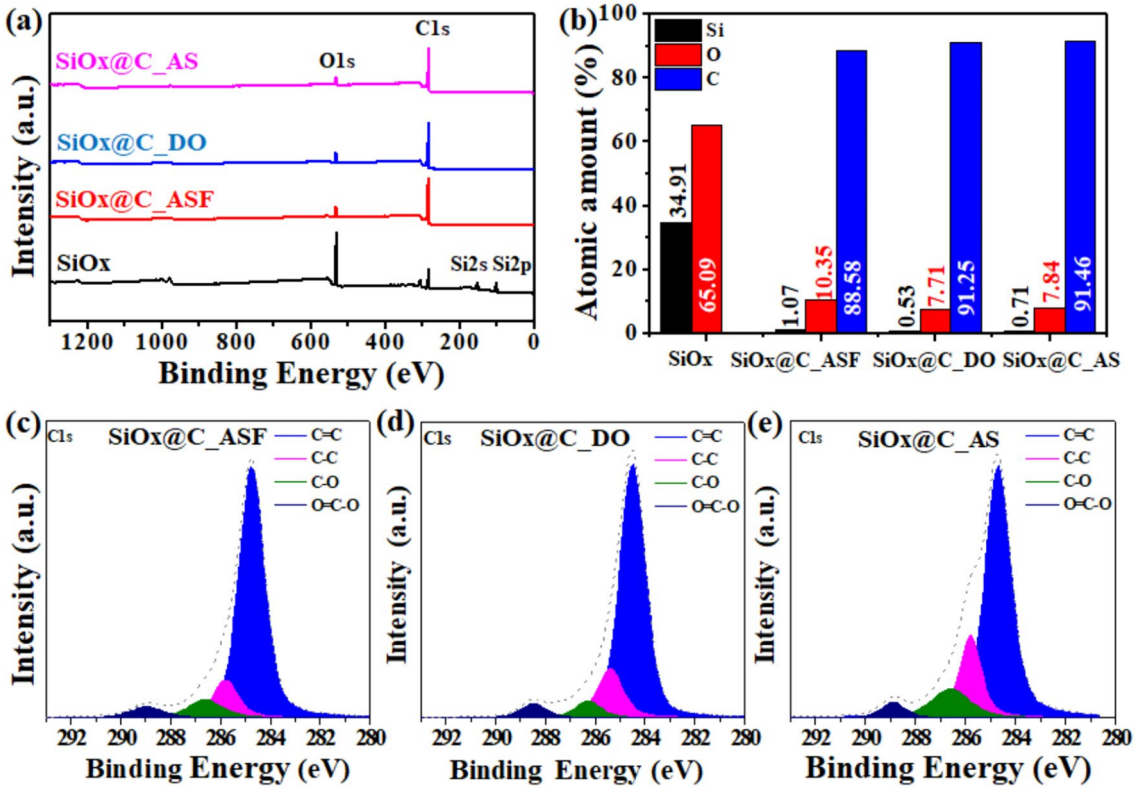

Fig. 3 (**a**) XPS survey spectra, (**b**) atomic percentages of SiOx, SiOx@C_ASF, SiOx@C_DO, and SiOx@C_AS, and XPS C 1s peak deconvolution of (**c**) SiOx@C_ASF, (**d**) SiOx@C_DO, and (e) SiOx@C_AS spectra

and 532.0 eV, respectively [51]. The XPS results for the SiOx carbon-coated with petroleum residues with different asphaltene contents were similar to the Raman results, as the Si 2p and Si 2s peaks were not observed, the oxygen content decreased, and the carbon content increased with increasing asphaltene content. On the other hand, the Si 2s peak was only observed in the uncoated SiOx, which had the highest oxygen content. The surface elemental content of the carbon-coated SiOx is shown in Fig. 3b. The significant decrease in Si upon coating SiOx with the petroleum residues suggested that the SiOx surface was evenly carbon-coated. In addition, the surface carbon content increased as the asphaltene content of the petroleum residue increased, which is believed to be due to the formation of a relatively crystalline carbon layer. To investigate the bonding structure and contents of carbon in the carbon layer of SiOx coated with petroleum residues with different asphaltene contents, the XPS C 1s spectrum peaks were divided into detailed peaks assigned to various bonding structures, as shown in Fig. 3c–e, and the peak functional groups and contents are shown in Table 1. Four peaks were observed in the C 1s spectrum, representing the bonds C = C, C–C, C–O, and O = C–O at 284.5, 285.4, 286.1, and 289.0 eV, respectively [52]. As the asphaltene content in the petroleum residue increased, the number of C = C bonds increased, while the number of C–C bonds decreased. It was confirmed that the asphaltene content in the petroleum residue affected the carbon layer generated on the SiOx surface, and it was determined that high-molecular-weight hydrocarbons such as asphaltene have a more crystalline structure than low-molecular-weight hydrocarbons.

Table 1 XPS C 1s deconvolution results of SiOx@C_ASF, SiOx@C_DO, and SiOx@C_AS

	SiOx@C_ASF	SiOx@C_DO	SiOx@C_AS
C = C	66.57	73.00	75.71
C–C	18.16	15.24	11.85
C–O	11.51	7.36	7.86
O = C–O	3.75	4.41	4.57

TEM analysis was used to determine the carbon layer thickness and microstructure of SiOx coated with petroleum residues with different asphaltene contents, and the results are shown in Fig. 4. Figure 4a shows that the SiOx contains no carbon surface layer, while Fig. 4b–d shows that a uniform amorphous carbon layer is formed on the surface of SiOx. As the asphaltene content of the petroleum residue increased, the thickness of the carbon coating layer tended to decrease to approximately 15.4 nm, 12.8 nm, and 8.1 nm, similar to findings from the Raman and XPS results. This is believed to occur due to a decrease in the number of components participating in the carbon layer formation process on the SiOx surface as the asphaltene content of the petroleum residue increases. To determine the carbon content

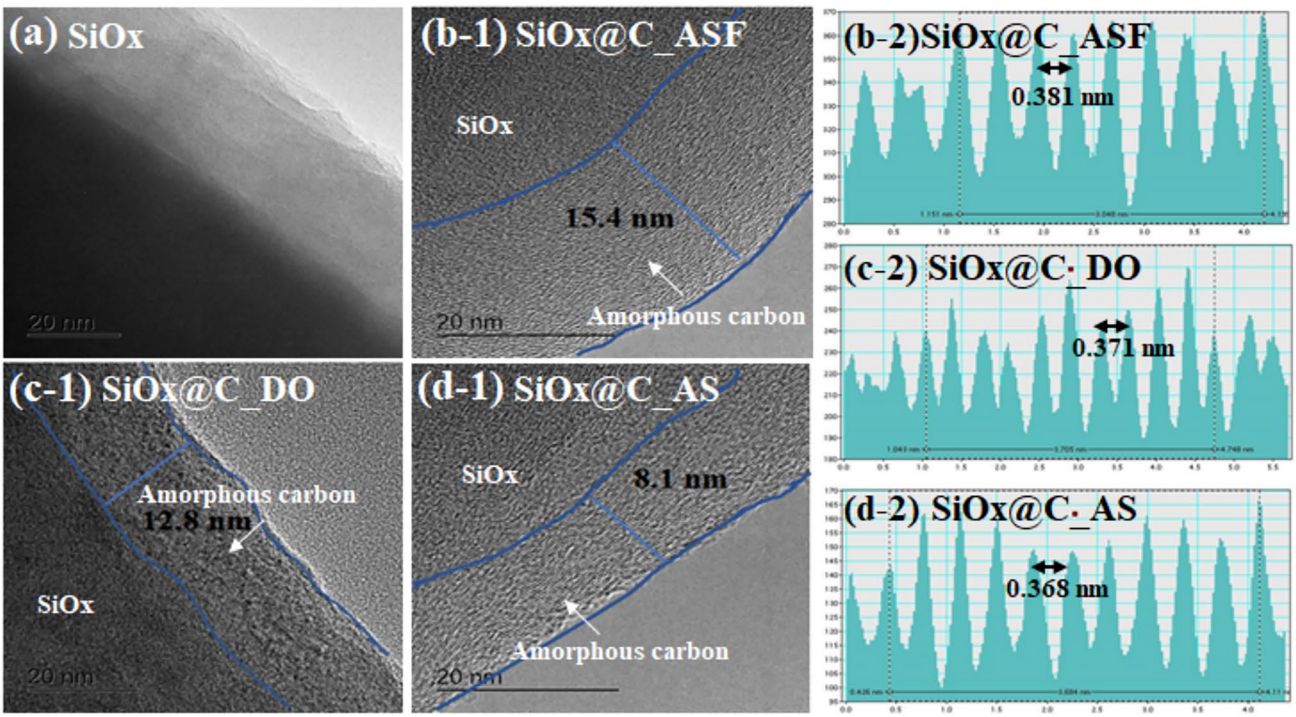

Fig. 4 TEM and IFFT images of (**a**) SiOx, (b) SiOx@C_ASF, (c) SiOx@C_DO, and (**d**) SiOx@C_AS

coated on the SiOx, TGA analysis was performed in an air atmosphere, the results of which are shown in Fig. S1. The analysis showed no weight loss of SiOx was observed, and the weight increased with increasing temperature, confirming the conversion of SiOx structure to SiO_2 structure [53]. The carbon coating layer is removed above 400 ℃ in an air atmosphere. The TGA retention of carbon-coated SiOx increased with the increase of asphaltene content, confirming that the carbon coating layer is relatively thin, which is similar to the results of previous TEM images and shows that under the same coating conditions, the asphaltene content of petroleum residue affects the thickness and crystallinity of the carbon coating layer depending on the components participating in the coating [54]. Figure 4b–d shows inverse fast fourier transform (IFFT) images of the carbon layer, and the d-spacing was calculated from the lattice pattern of the carbon layer as a function of the asphaltene content of the petroleum residues. With increasing asphaltene content in the petroleum residues, the d-spacings tended to decrease to 0.381 nm, 0.371 nm, and 0.368 nm. This confirmed that the crystallinity of the carbon layer improved with increasing asphaltene content in the petroleum residue, which is consistent with the Raman results. In addition, to observe the elemental distribution in the carbon layer, SiOx@C_ASF, SiOx@C_DO, and SiOx@C_AS were analyzed by energy dispersive X-ray spectroscopy (EDS), and the results are shown in Fig. S2a-c. EDS analysis revealed that carbon was evenly distributed on the surface of the Si particles, and SiOx@C_AS had a lower carbon content than SiOx@C_ASF. This suggests that polymeric hydrocarbons such as asphaltenes in the petroleum residues participate less in the carbon layer formation process, resulting in a relatively high crystallinity in the carbon layer due to axial polymerization of the components during the carbon lattice formation process, although the thickness of the carbon coating layer is thin.

3.3 Electrochemical performance of SiOx anodes carbon-coated with petroleum residues containing different asphaltene contents

To evaluate the electrochemical properties of SiOx and SiOx coated with petroleum residues of different asphaltene contents, charge/discharge, rate performance, and impedance experiments were performed, and the results are shown in Fig. 5. Figure 5a shows the charge/discharge profile for one cycle at a current density of 0.1 C. The SiOx and carbon-coated SiOx anodes showed similar charge–discharge curves. In the first cycle, SiOx, SiOx@C_ASF, SiOx@C_DO, and SiOx@C_AS exhibited discharge capacities of 411.2 mAh/g, 382 mAh/g, 404.2 mAh/g, and 415 mAh/g, respectively, with SiOx@C_AS exhibiting the highest discharge capacity. The discharge capacity decreased with increasing thickness of the carbon layer on the SiOx surface, and SiOx@C_AS exhibited the highest discharge capacity, which was attributed to the formation of a thin carbon layer. Furthermore, the initial efficiency of SiOx was 82.8%, and with increasing petroleum residual asphaltene content, the initial efficiency of the carbon-coated SiOx increased to 83.8, 84.8 and 85.5%, respectively. This suggests that the carbon coating of SiOx can improve the reversible capacity of lithium-ion batteries and that the thin and crystalline

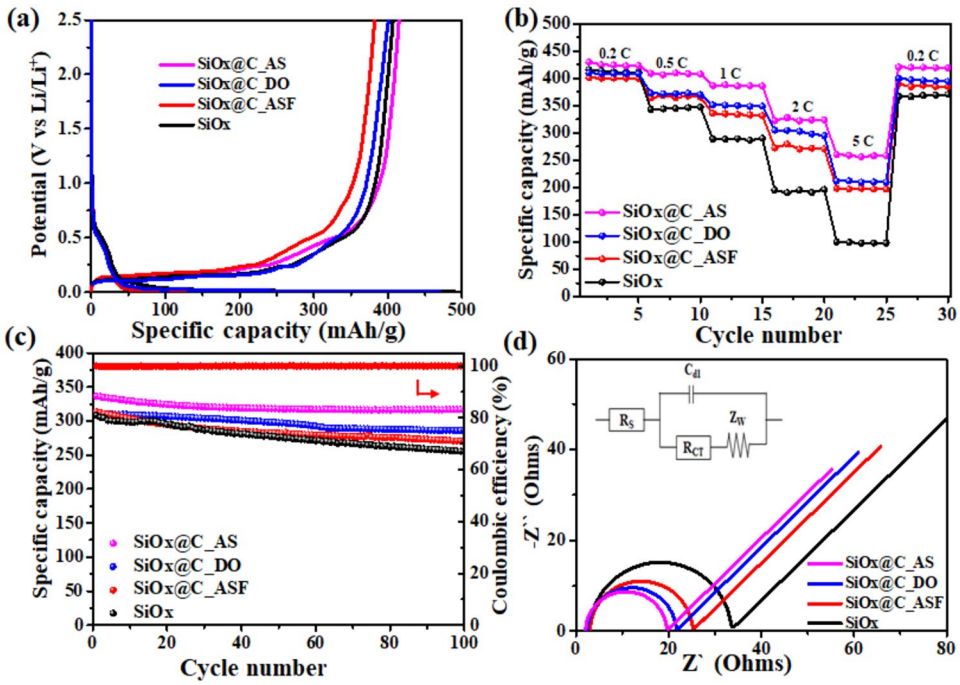

Fig. 5 Electrochemical properties of SiOx, SiOx@C_ASF, SiOx@C_DO, and SiOx@C_AS: (**a**) initial charge–discharge curves, (**b**) rate performance at various scan rates, (**c**) capacity retention at 1.0 C and (**d**) equivalent circuit and Nyquist plots

structure of the carbon layer formed by carbon coating with petroleum residue composed of polymeric hydrocarbons such as asphaltene facilitates the insertion and removal of lithium ions and forms a stable SEI layer.

To analyze the rate characteristics of the fabricated samples, C-rate analysis was performed by varying the current density, as shown in Fig. 5b. The current values for the C-rate test were obtained at different current densities of 0.2, 0.5, 1, 2, and 5 C. The capacity tended to decrease with increasing current density, with 425.0 mAh/g at 0.2 C, 408.3 mAh/g at 0.5 C, 386.7 mAh/g at 1 C, 324.1 mAh/g at 2 C, and 258.4 mAh/g at 5 C. SiOx@C_AS showed higher rate performance than SiOx, SiOx@C_ASF, and SiOx@C_DO. SiOx@C_AS showed the highest rate performance, with a rate retention of approximately 60.8% when the current density was increased from 0.2 C to 5 C. This is believed to have occurred due to the enhanced crystallinity of the asphaltene-based polymeric hydrocarbons in the carbon layer, which improved the conductivity of Li ions. In addition, after reaching a high current density, SiOx@C_AS showed a recovery of 98.8% to 420.0 mAh/g at 0.2 C, while SiOx showed a lower recovery of 89.3%, which was expected because the carbon coating based on petroleum residues prevented cracking of the SiOx electrode at high current densities. The better rate performance of SiOx@C_AS according to the increase in asphaltene content of petroleum residue can be explained using the diffusion coefficient of Li ions in the electrode. Therefore, cyclic voltammetry (CV) was performed to calculate the diffusion coefficient of Li ions. CV test was performed by changing the scanning speed from 0.2 to 1.0 mV/s to determine the Li diffusion coefficient (D_{Li^+}), and the results are presented in Fig. S3. The cathodic and anodic peak current (I_P) exhibits a linear relationship with the square root of the scanning rates, which can be used to characterize the Li-ion diffusion coefficients (D_{Li^+}) using Eq. (1) following the Randles–Sevcik equation [55].

$$I_P = \left(2.69 \times 10^5\right) n^{1.5} A D_{Li^+}^{0.5} \nu^{0.5} C_{Li^+} \quad (1)$$

where I_P is the peak current, n is the number of electrons transferred per reaction, A is the surface area of each electrode (1.5386 cm^2), D_{Li^+} is the Li diffusion coefficient, C_{Li+} is the Li-ion concentration in the electrolyte, and the ν is the scanning rate. Based on the above equation, the slope of the linear relationship between I_P and $\nu^{0.5}$ helps to estimate D_{Li^+} for each electrode. The Li-ion diffusion coefficient of SiOx@C_AS (2.04×10^{-8} cm^2/s for anode and 3.03×10^{-9} cm^2/s for cathode) shows a higher Li ion diffusion coefficient than that of SiOx@C_ASF (1.17×10^{-8} cm^2/s for anode and 1.17×10^{-9} cm^2/s for cathode). Through this, it is judged that as the asphaltene content of petroleum residue increases, Li-ion diffusion forms an advantageous carbon coating layer. The results for these Li-ion diffusion coefficients appear similar to the previous rate performance results and support excellent rate characteristics.

A comparison of the cycling stabilities of SiOx and carbon-coated SiOx is shown in Fig. 5c. After 100 cycles at 1.0 °C, the reversible capacities of SiOx, SiOx@C_ASF, and SiOx@C_AS were 255.1, 270.1, 285.9, and 316.9 mAh/g, respectively, and the capacity retention rates were 84.7, 88, 92, and 94.1%, respectively, after 100 cycles. The silicon oxide showed a decrease in reversible capacity at 100 cycles, which is believed to have occurred because the electrode could not withstand the volume change in the silicon oxide, leading to structural collapse. However, the SiOx carbon-coated with petroleum residue with asphaltene showed improved capacity retention, as the carbon layer buffered the volume expansion of the SiOx during the cycling process. Furthermore, the cycling stability improved as the asphaltene content of the petroleum residue increased. This occurred because the carbon layer formed from asphaltene was hard and elastic due to an increase in the number of C = C (SP^2) bonds and an increase in crystallinity, which mitigated the volume expansion of SiOx to form a stable SEI layer [41]. In addition, it was found that the carbon layer formed from asphaltene could accommodate the volume change; good cycling stability was obtained even after 100 cycles, although the layer had a lower thickness. To analyze the electrochemical behavior and diffusion coefficient during the insertion and desorption of lithium ions, we performed a galvanostatic intermittent titration technique (GITT) analysis, as shown in Fig. S4. The lithium-ion diffusion coefficient was calculated using Eq. (2), assuming that lithium-ion diffusion follows Fick's second law [50].

$$D_{Li^+} = \frac{4}{\pi\tau}\left(\frac{m_B V_M}{M_B S}\right)^2 \left(\frac{\Delta E_s}{\Delta E_\tau}\right)^2 \quad (2)$$

where m_B represents the mass of the electrode, Vm stands for the molal volume of the electrode, MB denotes the molecular weight of the electrode, A represents the area of the electrode, ΔE_s and ΔE_τ represent the amount of voltage change during constant current charging and the steady-state phase, respectively. During the GITT measurement, the cell was charged for 15 min at a normal current density of 1 C. There was also a 30 min resting period. It was confirmed that $D_{Li^+}(3.28 \rightarrow 12.89)$ of carbon-coated SiOx increased as the asphaltene content increased. Through this, the movement of lithium ions through the thin and crystalline carbon coating layer formed as the asphaltene content increases is advantageous, thereby improving lithium kinetics and thus improving rate characteristics.

To analyze the interfacial impedance of the fabricated samples, electrochemical impedance spectroscopy (EIS) was performed, and the results are shown in Fig. 5d. The fitted relevant elemental impedance values are shown in Table 2.

Table 2 The Concert parameters were obtained by fitting the EIS spectra of SiOx, SiOx@C_ASF, SiOx@C_DO, and SiOx@C_AS before cycling

	SiOx	SiOx@C_ASF	SiOx@C_DO	SiOx@C_AS
R_s	3.0	2.9	2.5	2.1
R_{ct}	30.3	22.0	19.1	17.4
Z_W	0.11	0.22	0.23	0.25

The Nyquist plot consisted of a semicircle in the high-frequency region representing the charge transfer resistance of the electrode–electrolyte interface and a straight line in the low-frequency region corresponding to the Warburg impedance of Li-ion diffusion. The SiOx carbon-coated with petroleum residues resulted in a smaller semicircle than SiOx, which confirmed that it had lower charge transfer resistance due to the carbon coating. This occurred because the carbon layer enhanced electrical conductivity on the SiOx surface. As shown in Table 2, the R_{ct} values are 30.3, 22.0, 19.1, and 17.4 Ω for SiOx, SiOx@C_ASF, SiOx@C_DO, and SiOx@C_AS electrodes, respectively. The SiOx@C_AS with the lowest charge transfer impedance can be attributed to the superior carbon coating layer and high electrical conductivity. Therefore, it is believed that the increased asphaltene content in the petroleum residue enhances the crystallinity of the carbon coating layer of the SiOx formed, resulting in improved electrical conductivity. This is similar to the trend for D_{Li^+} evaluated by GITT earlier, which may explain the excellent velocity characteristics. In general, the thick carbon layer and amorphous structure occur because it can hinder the migration of lithium ions, and the presence of a crystalline structure at the interface with the electrolyte can lower the electron transfer impedance. Therefore, a carbon layer with a thin and crystalline structure can be easily prepared by PVD-based carbon-coating on SiOx with petroleum residues containing high asphaltene contents to improve the electrochemical properties with high efficiency and high rate performance.

Surface and cross-sectional SEM images of electrodes before and after 100 cycles at 1 C were performed for deep insight into the effect of asphaltene content on the cycle performance of carbon-coated SiOx. As shown in Fig. S5, the surface of the electrode is smooth and dense without cracks before cycling, and the cross-sectional thickness of the electrode is 74.4 µm, 80.4 µm, 77.0 µm, and 79.4 µm, respectively. After 50 cycles, the thicknesses of the electrodes were 89.4 µm, 87.7 µm, 82.9 µm, and 84.2 µm, which were 20%, 9%, 7.6%, and 6% greater than the thickness of the electrodes before the cycle, respectively. Through this, the carbon coating layer with a high asphaltene content forms a more crystalline structure to alleviate the volume expansion of SiOx. Generally, when the change in electrode thickness is weak, the electrode layer adheres to the current collector and exhibits good cycle performance due to low internal resistance and volume expansion [56]. When the thickness of the electrode changes significantly, the aggregated SiOx particles on the electrode surface cause a huge volume expansion, and the contact between SiOx and the current collector is reduced or lost, resulting in poor electrochemical performance. It was confirmed that the structural stability of the SiOx@C-AS electrode was higher than that of the SiOx@C_ASF electrode. Therefore, SiOx with a high asphaltene content petroleum residue can form a carbon layer of the crystalline structure to mitigate the volume expansion of SiOx, thereby improving the electrochemical properties of high stability.

4 Conclusions

In summary, carbon-coated SiOx was prepared using petroleum residues with different asphaltene contents as the coating materials. The petroleum residues were categorized according to their asphaltene contents by solvent extraction. ASF consisted of low-molecular-weight hydrocarbons with no asphaltene, while AS consisted of high-molecular-weight hydrocarbons with high asphaltene content. The petroleum residues with different asphaltene contents formed an amorphous carbon layer on the SiOx surface. As the asphaltene content of the petroleum residue increased, the I_D/I_G ratio decreased, resulting in the formation of a crystalline carbon layer. On the other hand, when the content of asphaltene in the petroleum residue decreased, the carbon layer became thicker, but an amorphous carbon layer developed through evaporation and removal of the low-molecular-weight hydrocarbon components during heat treatment. SiOx@C_AS exhibited a greater discharge capacity (411.2 mAh/g at 0.2 C) and initial efficiency (85.5%) than did the other samples, and its rate performance improved at 0.2 C (425.0), 0.5 C (408.3), 1.0 C (386.7), 2.0 C (324.1), 5.0 C (258.4), and 0.2 C (420.0). This occurred because the SiOx@C_AS carbon layer was thin and highly crystalline; it buffered SiOx volume expansion and formed a stable SEI layer. In addition, the thin and highly crystalline structure of the carbon layer provided migration pathways for lithium ions, resulting in a high rate of performance. Therefore, the asphaltene content of petroleum residues can be adjusted through a simple pretreatment method to provide carbon precursors for preparing carbon-coated SiOx anode materials with high efficiency and high rate performance.

Supplementary Information The online version contains supplementary material available at https://doi.org/10.1007/s42823-024-00779-1.

Declarations

Conflict of interest No potential conflicts of interest relevant to this article were reported.

References

1. Xie L, Tang C, Bi Z, Song M, Fan Y, Yan C, Li X, Su F, Zhang Q, Chen C (2021) Hard carbon anodes for next-generation li-ion batteries: review and perspective. Adv Energy Mater 11:2101650. https://doi.org/10.1002/aenm.202101650
2. Zhang Y, Huang J, Saito N, Zhang Z, Yang L, Hirano S-I (2023) Search for stable host materials as low-voltage anodes for lithium-ion batteries: a mini-review. Energy Storage Mater 55:364–387. https://doi.org/10.1016/j.ensm.2022.11.030
3. Yuan S, Lai Q, Duan X, Wang Q (2023) Carbon-based materials as anode materials for lithium-ion batteries and lithium-ion capacitors: a review. J Energy Storage 31:106716. https://doi.org/10.1016/j.est.2023.106716
4. Liu K, Yang S, Luo L, Pan Q, Zhang P, Huang Y, Zheng F, Wang H, Li Q (2020) From spent graphite to recycle graphite anode for high-performance lithium ion batteries and sodium ion batteries. Electrochim Acta 356:136856. https://doi.org/10.1016/j.electacta.2020.136856
5. Zhang H, Yang Y, Ren D, Wang L, He X (2021) Graphite as anode materials: fundamental mechanism, recent progress and advances. Energy Storage Mater 36:147–170. https://doi.org/10.1016/j.ensm.2020.12.027
6. Li G, Ouyang T, Xiong T, Jiang Z, Adekoya D, Wu Y, Huang Y, Balogun MS (2021) All-carbon-frameworks enabled thick electrode with exceptional high-areal-capacity for Li-Ion storage. Carbon 174:1–9. https://doi.org/10.1016/j.carbon.2020.12.018
7. Kim KH, Cho JH, Hwang JU, Im JS, Lee YS (2021) A key strategy to form a LiF-based SEI layer for a lithium-ion battery anode with enhanced cycling stability by introducing a semi-ionic C-F bond. J Ind Eng Chem 99:48–54. https://doi.org/10.1016/j.jiec.2021.04.002
8. Dhamodharan D, Ghoderao PP, Dhinakaran V, Mubarak S, Divakaran N, Byun H (2022) A review on graphene oxide effect in energy storage devices. J Ind Eng Chem 106:20–36. https://doi.org/10.1016/j.jiec.2021.10.033
9. Cheng H, Shapter JG, Li Y, Gao G (2021) Recent progress of advanced anode materials of lithium-ion batteries. J Energy Chem 57:451–468. https://doi.org/10.1016/j.jechem.2020.08.056
10. Zhu GL, Zhao CZ, Huang JQ, He C, Zhang J, Chen S, Xu L, Yuan H, Zhang Q (2019) Fast charging lithium batteries: recent progress and future prospects. Small 15:1805389. https://doi.org/10.1002/smll.201805389
11. Blomgren GE (2019) The development and future of lithium ion batteries. J Electrochem Soc 164:A5019. https://doi.org/10.1149/2.0251701jes
12. Liu H, Sun Q, Zhang H, Cheng J, Li Y, Zeng Z, Zhang S, Xu X, Ji F, Li D, Lu J, Ci L (2023) The application road of silicon-based anode in lithium-ion batteries: from liquid electrolyte to solid-state electrolyte. Energy Storage Mater 55:244–263. https://doi.org/10.1016/j.ensm.2022.11.054
13. Liu X, Liu H, Cao Y, Wu X, Shan Z (2023) Silicon nanoparticles embedded in chemical-expanded graphite through electrostatic attraction for high-performance lithium-ion batteries. ACS Appl Mater Interfaces 15:9457–9464. https://doi.org/10.1021/acsami.2c21866
14. Casimir A, Zhang H, Ogoke O, Amine JC, Lu J, Wu G (2016) Silicon-based anodes for lithium-ion batteries: effectiveness of materials synthesis and electrode preparation. Nano Energy 27:359–376. https://doi.org/10.1016/j.nanoen.2016.07.023
15. Liu Z, Yu Q, Zhao Y, He R, Xu M, Feng S, Li S, Zhou L, Mai L (2019) Silicon oxides: a promising family of anode materials for lithium-ion batteries. Chem Soc Rev 48:285–309. https://doi.org/10.1039/C8CS00441B
16. Kim KS, Kang SC, Lee JD, Im JS (2021) Electrochemical performance of CB/SiOx/C anode materials by SiOx contents for lithium ion battery. Appl Chem Eng 32:117–123
17. Zhang K, Zhao D, Qian Z, Gu X, Yang J, Qian Y (2023) N-doped Ti3C2Tx MXene sheet-coated SiOx to boost lithium storage for lithium-ion batteries. Sci China Mater 66:51–60. https://doi.org/10.1007/s40843-022-2142-1
18. Xu Q, Sun JK, Yin YX, Guo YG (2018) Facile synthesis of blocky SiOx/C with graphite-like structure for high-performance lithium-ion battery anodes. Adv Funct Mater 28:1705235. https://doi.org/10.1002/adfm.201705235
19. Huang X, Lai G, Wei X, Liang J, Wu S, Ye KH, Chen C, Lin Z (2023) Scalable synthesis of SiOx-TiON composite as an ultrastable anode for Li-Ion half/full batteries. ACS Appl Mater Interfaces 16:26217–26225. https://doi.org/10.1021/acsami.4c03250
20. Lu H, Wang J, Liu B, Chu G, Zhou G, Luo F, Zheng J, Yu X, Li H (2019) Influence of carbon coating on the electrochemical performance of SiO@C/graphite composite anode materials. Chin Phys B 28:068201. https://doi.org/10.1088/1674-1056/28/6/068201
21. Guo J, Zhai W, Sun Q, Ai Q, Li J, Cheng J, Dai L, Ci L (2020) Facilely tunable core-shell Si@ SiOx nanostructures prepared in aqueous solution for lithium ion battery anode. Electrochim Acta 342:136068. https://doi.org/10.1016/j.electacta.2020.136068
22. Zhou X, Liu Y, Ren Y, Mu T, Yin X, Du C, Huo H, Cheng X, Zuo P, Yin G (2021) Engineering molecular polymerization for template-free SiOx/C hollow spheres as ultrastable anodes in lithium-ion batteries. Adv Funct Mater 31:2101145. https://doi.org/10.1002/adfm.202101145
23. Kuang S, Xu D, Chen W, Huang X, Sun L, Cai X, Yu X (2020) In situ construction of bamboo charcoal derived SiOx embedded in hierarchical porous carbon framework as stable anode material for superior lithium storage. Appl Surf Sci 521:146497. https://doi.org/10.1016/j.apsusc.2020.146497
24. Ouyang Q, Li G, Zhang X, Zhao X, Fu S, Li L (2023) Yolk-shell gradient-structured SiOx anodes derived from periodic mesoporous organosilicas enable high-performance lithium-ion batteries. Small 20:2305793. https://doi.org/10.1002/smll.202305793
25. Kim BR, Kim JH, Im JS (2022) Effect and mechanism of pitch coating on the rate performance improvement of lithium-ion batteries. Mater 15:4713. https://doi.org/10.3390/ma15134713
26. Hernandha RFH, Rath PC, Umesh B, Patra J, Huang CY, Wu WW, Dong QF, Li J, Chang JK (2021) Supercritical CO_2-assisted SiOx/carbon multi-layer coating on si anode for lithium-ion batteries. Adv Funct Mater 31:2104135. https://doi.org/10.1002/adfm.202104135
27. Ha S, Lim C, Myeong S, Lee IW, Lee YS (2024) Improvement of the electrochemical properties of Li/CFx primary batteries induced by nitrogen plasma treatment from silica and carbon fluoride. Carbon Lett 34:1521–1528. https://doi.org/10.1007/s42823-024-00719-z
28. Ha S, Lim C, Min CG, Myeong S, Ha N, Lee YS (2024) Improved energy and power density of a Li/CF_X primary battery through control of the C-F bonds with thermobaric modifications. J Ind Eng Chem 133:525–532. https://doi.org/10.1016/j.jiec.2023.12.029
29. Chae S, Xu Y, Yi R, Lim HS, Velickovic D, Li X, Li Q, Wang C, Zhang JG (2021) A micrometer-sized silicon/carbon composite anode synthesized by impregnation of petroleum pitch in

nanoporous silicon. Adv Mater 33:2103095. https://doi.org/10.1002/adma.202103095
30. Araño KG, Yang G, Armstrong BL, Aytug T, Chambers MS, Self EC, Meyer HM III, Quinn J, Browning JF, Wang C, Veith BM (2023) Carbon coating influence on the formation of percolating electrode networks for silicon anodes. ACS Appl Energy Mater 6:11308–11321. https://doi.org/10.1021/acsaem.3c02205
31. Kim D, Kim KH, Lim C, Lee YS (2022) Carbon-coated SiOx anode materials via PVD and pyrolyzed fuel oil to achieve lithium-ion batteries with high cycling stability. Carbon Lett. https://doi.org/10.1007/s42823-021-00314-6
32. Nolan D, Huang SW, Leskovsek V, Braun S (2006) Sliding wear of titanium nitride thin films deposited on Ti–6Al–4V alloy by PVD and plasma nitriding processes. Surf Coat Technol 200:5698–5705. https://doi.org/10.1016/j.surfcoat.2005.08.110
33. Kim KS, Hwang JU, Lim JS, Lee JD, Kim JH, Kim MI (2020) The effect of waste PET addition on PFO-based anode materials for improving the electric capacity in lithium-ion battery. Carbon Lett 30:545–553. https://doi.org/10.1007/s42823-020-00124-2
34. Han YJ, Hwang JU, Kim KS, Kim JH, Lee JD, Im JS (2019) Optimization of the preparation conditions for pitch based anode to enhance the electrochemical properties of LIBs. J Ind Eng Chem 73:241–247. https://doi.org/10.1016/j.jiec.2019.01.031
35. Seo SW, Kim JH, Lee YS, Im JS (2018) Identification of synthesized pitch derived from pyrolyzed fuel oil (PFO) by pressure. Appl Chem Eng 29:652–656
36. Lim C, Jeong SG, Ha N, Myeong S, Min CG, Yu Y, Yang X, Lee YS (2024) Plasma-mediated F-doped activated carbon embedded with N and S atoms for the effective removal of CO_2 gas. J Ind Eng Chem. https://doi.org/10.1016/j.jiec.2024.06.015
37. Ha S, Hwang K, Kim D, Yoon S, Lee YS (2023) Multiple performance enhancements with one effect: improving the electrochemical performance of SiOx coated with specific aromatic compounds. J Ind Eng Chem 25:188–19510
38. Ming L, Dong L, Zhuowu M, Bin L, Shitao Y, Junwei D, Wenlong C (2018) Effects of different extracted components from petroleum pitch on mesophase development. Fuel 222:617–626. https://doi.org/10.1016/j.fuel.2018.03.011
39. Long G, Yonggang W, Yiting Z, Jingdong Y, Haiyong Z, Xiongchao L (2023) The effect of n-heptane soluble content on the composition and structure of coal tar pitch and the preparation of needle coke. J Anal Appl Pyrolysis 175:106201. https://doi.org/10.1016/j.jaap.2023.106201
40. Alostad LK, Lonzano DCP, Gannon B, Downham RP, Jones HE, Barrow MP (2022) Investigating the influence of n-heptane versus n-nonane upon the extraction of asphaltenes. Energy Fuels 36:8663–8673
41. Wen T, Fan Y, Tingting Y, Gang L, Xiaoting W, Qiurong L, Yi L, Yingzhi L, Chuanfei G, Kun L, Zhouguang L, Qingxia L, Zhenghe X (2022) Fullerene-like elastic carbon coatings on silicon nanoparticles by solvent controlled association of natural polyaromatic molecules as high-performance lithium-ion battery anodes. Energy Storage Mater 45:412–421. https://doi.org/10.1016/j.ensm.2021.11.040
42. Ferreira RdM, Almeida MOQd, Chrisman ECAN, Ribeiro BD, Coelho MAZ (2023) Cold extraction of post-salt oil asphaltenes and their solubilization in deep eutectic solvents. Chem Eng Res Des 198:349–356. https://doi.org/10.1016/j.cherd.2023.09.015
43. Kim JG, Kim JH, Song BJ, Jeon YP, Lee CW, Lee YS, Im JS (2019) Characterization of pitch derived from pyrolyzed fuel oil using TLC-FID and MALDI-TOF. Fuel 167:25–30. https://doi.org/10.1016/j.fuel.2015.11.050
44. Nguyen NT, Park S, Jung J, Cho J, Lee CW, Park Y (2018) Comparative reactivity between thermal and catalytic hydrocracking of vacuum residue: effect of asphaltenes. J Ind Eng Chem 61:32–38. https://doi.org/10.1016/j.jiec.2017.11.044
45. Lim C, Ha S, Myeong S, Ha N, Min CG, Lee YS (2024) Production of needle cokes via mild condition co-pyrolysis of FCC-DO and PFPE. Fuel 360:13622. https://doi.org/10.1016/j.fuel.2023.130622
46. Lim C, Ko Y, Kwak CH, Kim S, Lee YS (2022) Mesophase pitch production aided by the thermal decomposition of polyvinylidene fluoride. Carbon Lett 32:1329–1335. https://doi.org/10.1007/s42823-022-00369-z
47. Seo SW, Ahn WJ, Kang SC, Im JS (2024) Effect of pitch crystallinity on electrochemical performance of graphite carbon coatings. J Energy Storage 81:110489. https://doi.org/10.1016/j.est.2024.110489
48. Dong H, Wang J, Ding H, Wang P, Song R, Zhang N, Li F, Li S (2021) The mosaic structure design to improve the anchoring strength of SiOx@C@Graphite anode. Mater Today Chem 22:100599. https://doi.org/10.1016/j.mtchem.2021.100599
49. Jin C, Dan J, Zou Y, Xu G, Yue Z, Li X, Sun F, Zhou L, Wang L (2021) Carbon-coated nitrogen doped SiOx anode material for high stability lithium ion batteries. Ceram Int 47:29443–29450. https://doi.org/10.1016/j.ceramint.2021.07.112
50. Seo SW, Ahn WJ, Lee YS, Kang SC, Im JS (2023) Improvement of capacitor performance by pitch-based binder for a new alternative to polymer binders. Surf Interfaces 37:102726. https://doi.org/10.1016/j.surfin.2023.102726
51. Ren Z, Liu S, Chen J, Yu Y, Shang Q, Fakudze S, Liu C, Zhou P, Chu Q (2022) One-step synthesis of interface-coupled Si@SiO_X@C from whole rice-husks for high-performance lithium storage. Electrochim Acta 402:139556. https://doi.org/10.1016/j.electacta.2021.139556
52. Kim KH, Kang DH, Kim MJ, Lee YS (2019) Effect of C-F bonds introduced by fluorination on the desalination properties of activated carbon as the anode for capacitive deionization. Desalination 457:1–7. https://doi.org/10.1016/j.desal.2018.12.005
53. Kang W, Zhang Q, Jia Y, Liu X, Jiang N, Zhao Y, Wu C, Guan L (2024) Enhancing the cycling stability of commercial silicon nanoparticles by carbon coating and thin layered single-walled carbon nanotube webbing. J Energy Storage 602:234338. https://doi.org/10.1016/j.jpowsour.2024.234338
54. Murugananthan R, Yang CH, Wang HJ, Huang CH, Liu WR (2022) Industrial silicon-wafer-wastage-derived carbon-enfolded Si/Si-C/C nanocomposite anode material through plasma-assisted discharge process for rechargeable Li-Ion storage. Nanomaterials 12:659. https://doi.org/10.3390/nano12040659
55. Im J, Kwon DH, Kim DH, Yoon S, Cho KY (2021) P-doped SiOx/Si/SiOx sandwich anode for Li-Ion batteries to achieve high initial coulombic efficiency and low capacity decay. Small Methods 6:2101052. https://doi.org/10.1002/smtd.202101052
56. Wang F, Lin S, Lu X, Hong R, Liu H (2022) Poly-dopamine carbon-coated stable silicon/graphene/CNT composite as anode for lithium ion batteries. Electrochim Acta 404:139708. https://doi.org/10.1016/j.electacta.2021.139708